UNCECOMP 2015
1st ECCOMAS Thematic Conference on
Uncertainty Quantification in Computational Sciences and Engineering
M. Papadrakakis, V. Papadopoulos, G. Stefanou (eds.)
Crete Island, Greece, 25–27 May 2015

MATHEMATICAL MORPHOLOGY AND UNCERTAINTY QUANTIFICATION APPLIED TO THE STUDY OF DUAL PHASE STEEL FORMATION

Alessandra Micheletti[1,2], Junichi Nakagawa[3], Alessio A. Alessi[1], Vincenzo Capasso[2], Daniela Morale[1], Elena Villa[1]

[1] Dept. of Mathematics, Università degli Studi di Milano
via Saldini 50, Milano, Italy
email: {alessandra.micheletti, alessio.alessi, daniela.morale, elena.villa}@unimi.it

[2] ADAMSS Centre, Università degli Studi di Milano
via Saldini 50, Milano, Italy
email: vincenzo.capasso@unimi.it

[3] Mathematical Science & Technology Research Lab, Nippon Steel & Sumitomo Metal Corporation,
20-1 Shintomi, Futtsu-City, Chiba, 293-8511, Japan,
email: nakagawa.q9p.junichi@jp.nssmc.com

Keywords: Germ grain model, mathematical morphology, dual phase steel, uncertainty quantification

Abstract. *Dual Phase steels (DP steels) have shown high potential for automotive and other applications, due to their remarkable property combination between high strength and good formability. The mechanical properties of the material are strictly related with the spatial distribution of the two phases composing the steel, ferrite and martensite, and their stochastic geometry. Unfortunately the experimental costs to obtain images of sections of steel samples are very high, thus one important industrial problem is to reduce the number of 2D sections needed to reconstruct or simulate in a realistic way the 3D geometry of the material. This reduction causes an increase of the uncertainty in the parameters estimates of suitable geometric models for the material.*

In this work we present an approach based on the definition of a germ-grain model which approximates the main geometric characteristics of the martensite. The parameters of the model are estimated on the basis of the morphological characteristics of the images of about 150 tomographic sections of a real sample, and plausibility regions for the estimated parameters are computed. The increase in uncertainty on the parameters estimates in presence of a reduced number of sections is then quantified in terms of increase in the volume of the corresponding plausibility regions. Even though the model still needs some improvements in the fitting with the real data, the overall procedure for uncertainty quantification that we have obtained can be generalized to other study cases and can be used by the industry to set up a suitable experimental plan to fit a model to the data with a desired accuracy.

1 Introduction

Dual Phase steels (DP steels) have shown high potential for many applications due to their remarkable property combination between high strength and good formability.

Here we consider a sample of steel formed by martensite and ferrite. The relative position and geometric structure of the two phases is responsible of the mechanical properties of the material, thus it is particularly important to provide statistical models which may reproduce the main geometric characteristics of the two phases. Our results are based on images of about 150 tomographic sections taken from a lab sample of steel.

The formation of the two phases of the material starts after a cooling phase of the melted alloy of iron and carbon, during which austenite is formed, followed by a rolling phase, transforming slabs of steel into thin metal foils.

A further cooling phase follows the rolling; during this phase the formation of ferrite starts. Crystals of ferrite nucleate mainly from the interfaces of the rolled (and thus deformed) austenite, and grow up to impingement with other crystals of ferrite, driven by the evolving field of carbon concentration. After a fixed time interval the formation of ferrite is stopped by a sudden quenching, during which the material still not transformed into ferrite becomes martensite. The final result is a dual phase steel formed by ferrite and martensite, having a stochastic geometric structure.

In order to define a dynamical model able to reproduce the complete geometric structure of the material, a stochastic birth and growth process coupled with the evolution of the carbon field should be used (see [1] for similar models applied to polymer crystallization). A first model which goes in this direction, though facing the problem at only a macroscopic scale, has been studied in [7].

In the following we will introduce a possible approach to reproduce the main mean geometric characteristics of the martensite contained in the real sample via a germ-grain model. The model requires further improvements in order to obtain a better agreement with the real data, as will be clear from our results. Anyway this is a proposal of a general procedure that may be applied to this and to other similar case studies in which the reduction of the experiments and measurements to study the random geometry of the material, without loosing too much information, is a crucial industrial issue.

As from a confidentiality agreement with Nippon Steel & Sumitomo Metal, who provided the real data, the images of the real sample will not be shown.

2 Structure of the austenite phase

First of all we studied the geometric structure of the interfaces of austenite after rolling, since nucleation of ferrite happens mainly on such interfaces, so that the location of the final ferrite and martensite crystals depends on the location of such interfaces.

The shape of the crystals of austenite before rolling is quite close to a 3D Voronoi tessellation. The rolling reduces the thickness of the rolled slab to 1/50 of the original thickness, but preserving the width and the total volume. The result is a long thin foil (see Figure 1).

If we apply a deformation to a 3D Voronoi tessellation, maintaining the proportions used in the real experimental situation, we obtain the results shown in Figure 2.

Since the real sample is composed of a very small portion of the rolled metal foil, extracted from the middle of the foil, we sectioned a small cube of the deformed tessellation, with dimensions proportional to the real sample, in order to look at its internal geometric structure. Two sections in the x_1x_3 and x_2x_3 directions, respectively, are reported in Figure 3.

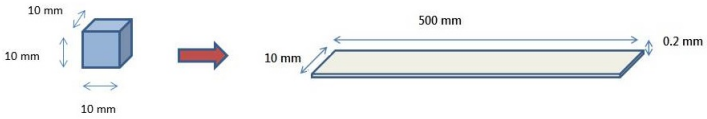

Figure 1: Deformation applied to the cube containing the 3D Voronoi tessellation formed by austenite crystals

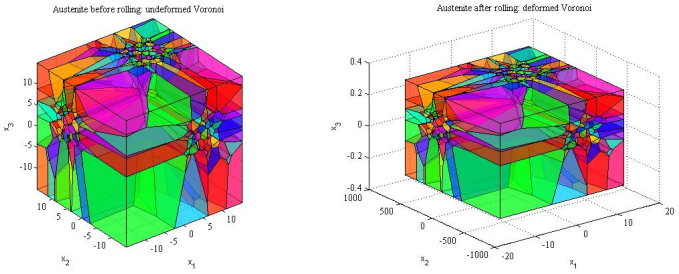

Figure 2: Voronoi tessellation of the 3D space with 3000 crystals in a cube. On the left: before rolling, on the right: after rolling. The different axes scales in the two images evidentiate the defonrmation along the three axes, due to rolling

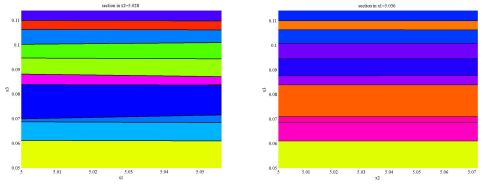

Figure 3: Two sections of the deformed Voronoi tesselation on the right of Figure 2, taken in the center of the parallelepiped. On the left: section parallel to the x_1x_3 plane; on the right: section parallel to the x_2x_3 plane. Different colours correspond to different crystals

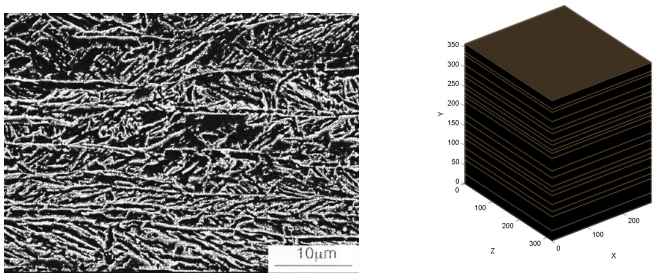

Figure 4: On the left: pancake structure image of austenite after rolling and before the birth and growth of ferrite; on the right: simulated random parallel planes, with an inhibition distance, from which the nucleation of ferrite starts

It is evident that, at the scales relevant for our application, the effect of rolling is the transformation of the interfaces of the 3D Voronoi tessellation into approximately parallel planes, having random quotes along the x_3 axis. The distribution of the quotes looks quite regular. This is in accordance with the images of sections of austenite after rolling, which shows a typical pancake structure (see Figure 4) and with applications to other materials already studied in literature [8].

We have thus modelled the interfaces of austenite as parallel horizontal planes, i.e. parallel to direction x_1x_2, with randomly distributed quotes along the x_3 axis. The quotes have been distributed according to a 1-dimensional hard core process [2, Section 5.4], that is a point process with an inhibition distance between points. Figure 4 on the right shows a simulated realization of such a process.

In Figure 5 a simulated sample of the two phases which resembles the real one is reported. The black region, occupied by martensite, can be represented as the free space between different crystals of ferrite at the moment of quenching. Since the crystals of ferrite nucleate on the parallel planes representing the interfaces of austenite, martensite will have a tendency to concentrate in between two adjacent parallel planes.

3 Morphological analysis of the martensite

In order to set up a geometrical model which may realistically represent the material, we first described quantitatively the geometrical structure of the martensite via a morphological analysis of the real sample. The morphology of a random set may be described by the densities of the Minkowski functionals (see [2] for the definition). In particular we concentrated on the volume density V_V (fraction of the volume occupied by the random set), the surface density S_V (surface of the random set per unit volume), and the density of Euler-Poincaré characteristics E_V (number of connected components of the random set per unit volume). In general these functionals are constant in space only if the random set under study is isotropic and stationary, i.e. its distribution is invariant under rigid motions.

We computed the Minkowski functionals of the martensite of the real sample, by sectioning the sample into slices of 10 voxels of width in the three main directions, in order to test also the presence of zones of non stationarity or of anisotropies. The functionals have been computed according to the estimators described in [3], using the Matlab codes which can be downloaded from [4]. The results are reported in Figure 6. The functionals look almost constant along the directions Z and X, while V_V and S_V show a periodicity along the direction Y (see Figure 5 for the names of the directions). This fact is confirmed by a visual inspection of the real sample,

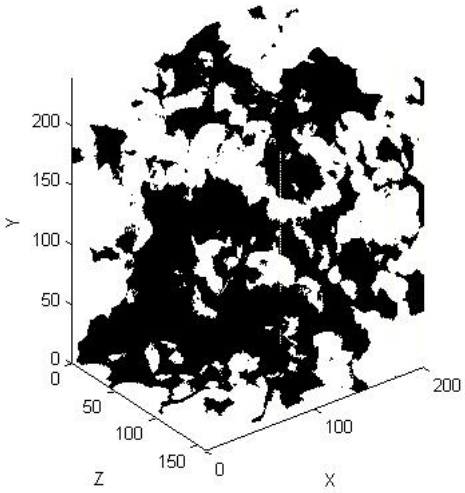

Figure 5: A simulated sample of the two phases: the region occupied by martensite is depicted in black, while ferrite is in white.

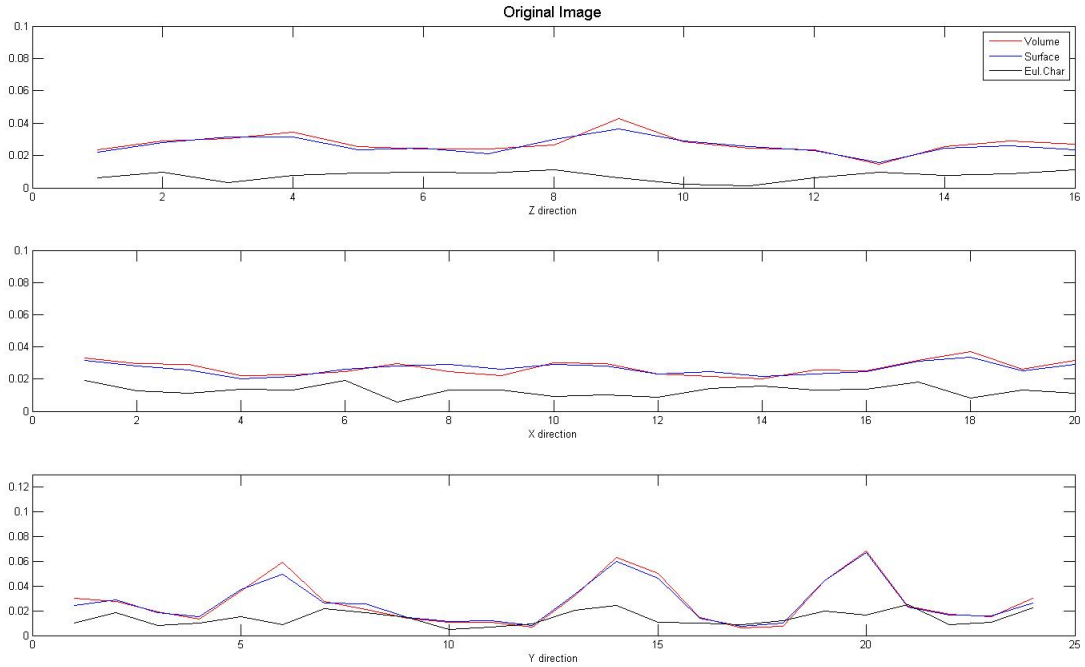

Figure 6: The Minkowski functionals computed on the real sample along the three main directions. The directions have been named like in Figure 5

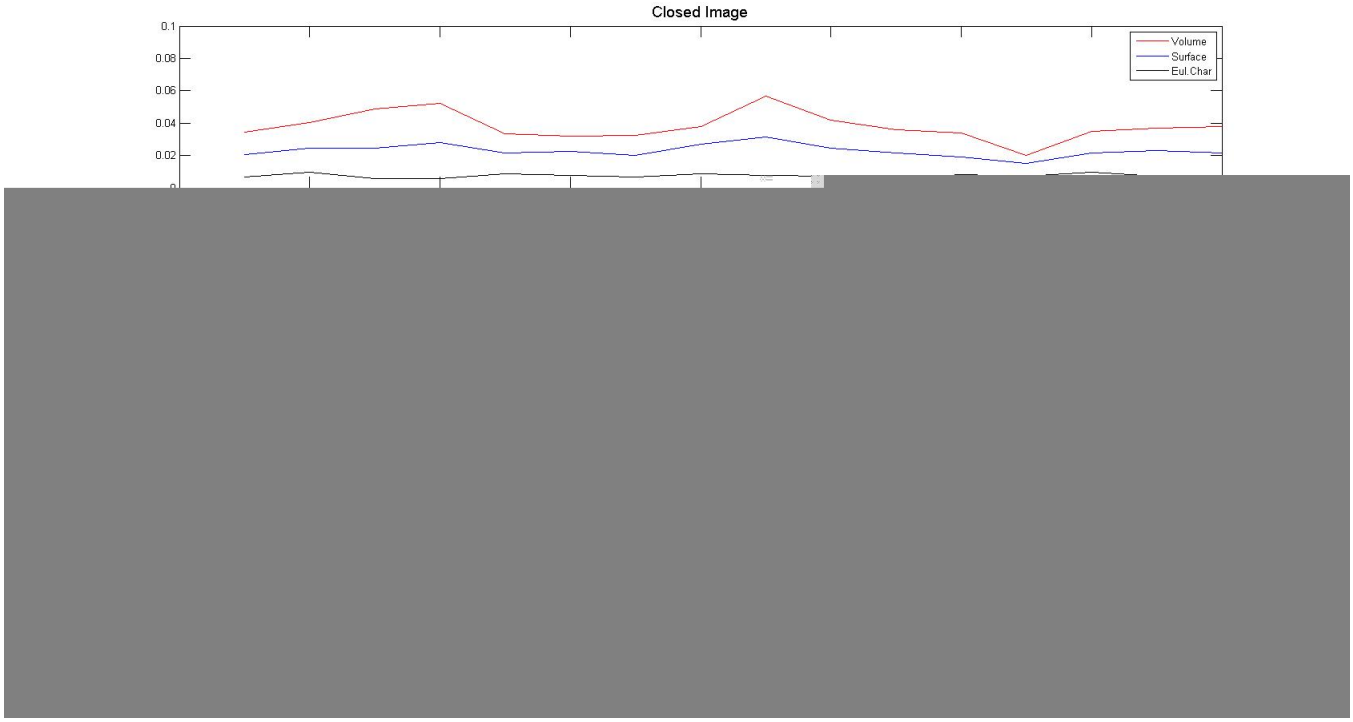

Figure 7: The Minkowski functionals computed along the three main directions on the real sample after a closing with a sphere of radius 5 voxels. The directions have been named like in Figure 5

which shows a ”striped” structure in direction Y, which is coherent since the direction of rolling is parallel to the XZ plane and thus the crystals of ferrite are born on planes parallel to the XZ plane.

We also deduce from the graphics that the martensite is very ”fragmented”, in particular observing the behaviour of the surface density and the volume density, which are almost overlapped in all directions. This is confirmed by a visual inspection of the real sample, since many small holes or pores are present in the material and the martensite in some places is needle shaped. This porosity does not influence much the mechanical properties of the material, thus it can be neglected in the construction of a realistic geometric model. Since the presence of the pores can not be easily reproduced with a geometrical germ-grain model, we performed a closure of the 3D real sample [6], with a sphere of 5 voxels of radius. The closure of a random set has the effect of ”filling the small holes”. The Minkowski functionals of the closed image are reported in Figure 7. Now the volume and surface density are different, because of the lower fragmentation of the image.

We will use the closed image and its Minkowski functionals as a reference in the procedure of parameter identification of the geometrical model reproducing the material, described in the following sections.

4 A germ-grain model

In order to set up a statistical model able to reproduce the mean geometric structure of the real sample of steel, we have proposed a germ-grain model with spherical grains, depending on a small set of unknown parameters. The model will reproduce the structure of the ferrite phase, neglecting the interfaces between different crystals, so that the martensite will be represented

by the empty space between different grains of the model.

A germ-grain model is a random closed set $\Xi \subseteq \mathbb{R}^d$ defined as

$$\Xi = \cup_{i \in \mathbb{N}} \Theta_i \oplus x_i$$

where $\{x_i\}$ are points in $\mathbb{R}^d$ forming a locally finite point process, called *germs*; Θ_i are i.i.d. uniformly bounded random closed sets (usually containing the origin) called *grains*, and $\oplus$ denotes the Minkowski sum between sets, thus $\Theta_i \oplus x_i = \{y + x_i | y \in \Theta_i\}$ (for more details see [5, 2]).

We modelled the point process of germs as a Neyman-Scott clustered point process, taking into account that ferrite nucleates in the surrounding of parallel planes, and also observing that martensite in the real sample exhibits a "striped" structure.

The Neyman-Scott point process [2, Section 5.3] is formed by generating a spatial Poisson point process of *parents* having intensity $\lambda_p(x)$ and then surrounding the parents by a random number of *daughter points*, scattered independently and identically distributed around the parents. The parents are then removed and the Neyman-Scott process is formed just by the daughter points.

The germs in our model have thus been generated according to the following algorithm:

Algorithm 1

Input:

n_{planes} = number of parallel planes,

σ_{vert}= standard deviation of the daughters'distribution in the vertical direction,

σ_{hor}= standard deviation of the daughters'distribution in the horizontal direction,

λ=mean number of germs to be generated

step 1: randomly generate a set of parallel planes, from which ferrite nucleates;

step 2: generate the number $N_g \sim Poisson(\lambda)$ of germs to be located in the 3D space

step 3: fix the number of parent germs to $\frac{N_g}{4}$

step 4: distribute the parent germs uniformly on the parallel planes

step 5: distribute the N_g daughter germs around the parents according to a 3-variate normal distribution having diagonal covariance matrix given by

$$\Sigma = diag(\sigma^2_{hor}, \sigma^2_{hor}, \sigma^2_{vert}).$$

The grains have been modeled as independent spheres of random radius $R = L \cdot \rho$, where L is a constant representing the maximum possible radius of the spheres and ρ is a random variable distributed as a mixture of two Beta distributions, as follows:

- $\rho \sim Beta(3, b1)$ with $b1 > 3$ with probability 0.7 (favouring small radii),
- $\rho \sim Beta(3, b2)$ with $b2 < 3$ with probability 0.3 (favouring big radii).

This choice has been motivated by an analysis of the granulometry of the material [6], which provides such proportions of "big" and "small" grains.

In order to avoid edge effects, the simulation of the model has been performed in a window of observation enlarged by L on each side, and then only the central portion of the window

Parameter	optimal value
n_{planes}	12
σ_{hor}	9.6386
σ_{vert}	14.1081
L	16
$b1$	4.7173
$b2$	1.376
λ	10020

Table 1: Optimal values of the parameters. The corresponding computed Mahalanobis distance is 2.34. The simulations have been performed in a parallelepiped having the same dimensions of the real sample, where the side of each voxels is $0.25\mu m$ long. The unit of measure of the parameters is a voxel side length

with dimensions equal to the real sample has been considered. All the simulations have been performed in Matlab.

Thus our germ grain model is based on the following seven parameters:

$$(n_{planes}, \sigma_{hor}, \sigma_{vert}, L, b1, b2, \lambda) \in \mathbb{N} \times \mathbb{R}_+ \times \mathbb{R}_+ \times \mathbb{N} \times [3, +\infty) \times (0, 3) \times (0, +\infty) \quad (1)$$

5 Parameters estimates

For each set of the parameters $\underline{p} = (n_{planes}, \sigma_{hor}, \sigma_{vert}, L, b1, b2, \lambda)$ we performed 10 simulations of the germ grain model, and on each simulation we computed the volume, surface, mean and Euler characteristic densities (i.e. the densities of Minkowski functionals). The parameters can be estimated by minimizing a suitable distance between the values of the densities measured on the (closed) real sample and the densities of the simulated germ-grain model.

Let us denote by $\underline{S}_{real} \subseteq \mathbb{R}^3$, the densities of the three functionals estimated on the real sample, by $\bar{\underline{S}}_{sim}(\underline{p}) \subseteq \mathbb{R}^3$ the means, over 10 simulations, of the densities of the three functionals computed on the simulated samples, and by $\hat{\Sigma}$ the sample covariance matrix of the densities computed on the simulations.

In order to minimize with respect to the parameters $\underline{p}$, we have adopted the *Mahalanobis distance*, given by

$$\Delta(\underline{S}_{real}, \bar{\underline{S}}_{sim}(\underline{p})) = \sqrt{(\underline{S}_{real} - \bar{\underline{S}}_{sim}(\underline{p}))^T \hat{\Sigma}^{-1} (\underline{S}_{real} - \bar{\underline{S}}_{sim}(\underline{p}))},$$

since it weighs the distance from the mean of the simulations with respect to the variance, taking thus into account the variability related with each set of parameters. Note that the distance (5) is stochastic, being based on the outcomes of random simulations.

Since both parameters n_{planes} and L are integers (the maximum radius of the spheres has been defined in the simulation program in terms of number of voxels), we needed to apply an optimization algorithm to a function which is not expressed in algebraic form and depending upon mixed integer and real parameters, so that we have decided to apply a genetic algorithm for the best fitting

$$\hat{\underline{p}} = \arg\min_{\underline{p}} \Delta(\underline{S}_{real}, \bar{\underline{S}}_{sim}(\underline{p})).$$

The estimated parameters are reported in Table 1.

We have performed numerical simulations of the sample using the estimated optimal parameters, and computed the densities of the relevant Minkowski functionals on the simulated

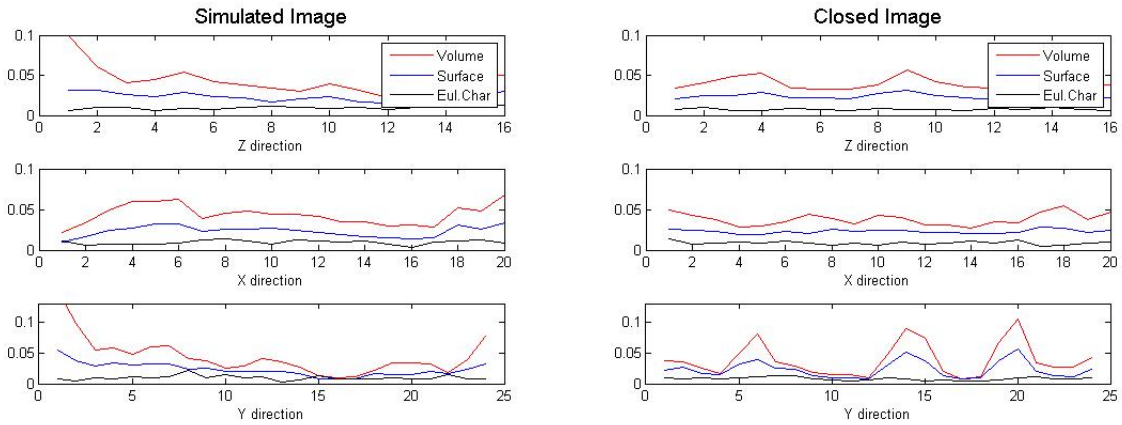

Figure 8: Comparison of the densities of Minkowski functionals between a simulation performed with the optimal parameters reported in Table 1 and the closed true image

Parameter	optimal value
n_{planes}	5 fixed
σ_{hor}	9.06
σ_{vert}	17.73
L	16
$b1$	9.34
$b2$	1.38
λ	10564

Table 2: Optimal values of the parameters fixing the number and location of nucleation planes

sample. The results are shown in Figure 8. Unfortunately, even though the numerical agreement between real data and simulated data is rather satisfactory in terms of orders of magnitude, our simulations do not capture detailed features such as the periodicity of volume and surface densities along the Y axis.

We then tested a second model where we fixed at 5 the number of parallel planes from which ferrite originates, located ”in the valleys” between two peaks in the graph referring to Y direction in Figure 7. This choice is due to the fact that in our model martensite occupies the space left free by ferrite, thus the peaks in volume and surface densities of the martensite will be located in between two nucleation planes of ferrite. All the other parameters have been estimated via the optimization procedure described above. The results are reported in Table 2. The Minkowski functionals computed on a simulated image with the new optimal parameters are compared with those of the closed true image in Figure 9. As above, in this case too the observed periodicity along the Y axis has not been captured.

This motivates future directions of research by including additional realistic ingredients in the proposed statistical geometric model. A possible improvement could be obtained by changing the shape of the primary grain to an ellipsoid, since the grains of ferrite are often elongated, and thus are poorly approximated by spheres. In this case, a preliminary study of the distribution of the sizes of the three main diameters of the ellipsoids should be performed.

For the time being we will concentrate first in performing a sensitivity analysis of the param-

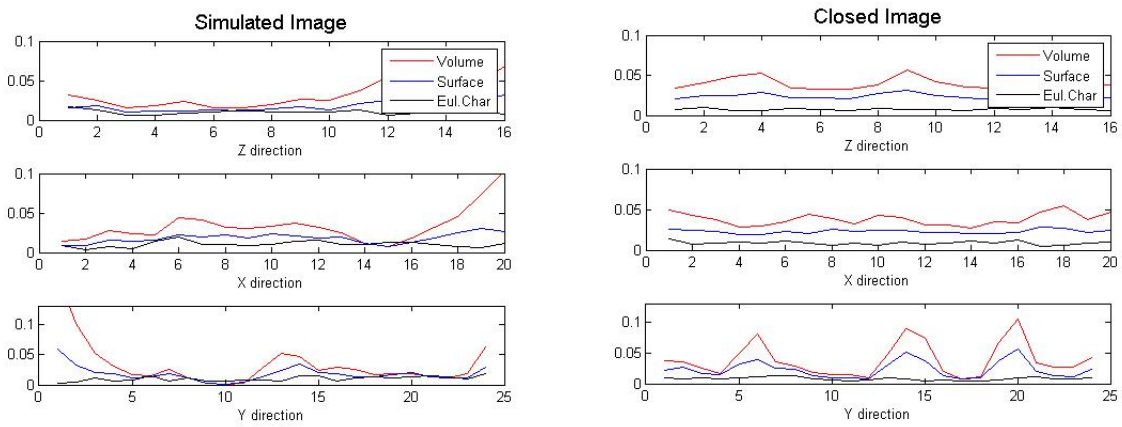

Figure 9: Comparison of the densities of Minkowski functionals between a simulation performed with the optimal parameters reported in Table 2 and the closed true image

Parameter	exploration interval
n_{planes}	$[4, 6]$
σ_{hor}	$[7.25, 10.87]$
σ_{vert}	$[14.18, 21.28]$
L	$[13, 19]$
$b1$	$[7.47, 11.21]$
$b2$	$[1.1, 1.66]$
λ	$[8451, 12677]$

Table 3: Intervals of variation of each parameter in the sensitivity analysis. The integer parameters n_planes and L have explored only the integer values contained in the respective intervals, the other parameters have explored 10 equally spaced points inside each interval

eters of our model, which will be taken into account in the formulation of more realistic models, and then in evaluating the increase of uncertainty due to a reduction of the sample size (i.e. of the number of sections on the experimental sample).

6 Sensitivity analysis

In order to understand which parameters have a bigger influence on the variability of the densities of Minkowski functionals, we performed a sensitivity analysis as follows. We made one parameter at a time vary in an interval centered in the optimal value reported in Table 2, fixing all the other parameters equal to the optimal values. We explored a variation of about the 20% of the value of each parameter, as reported in Table 3.

For each value of the parameters we performed 15 simulations, on each simulated image we computed the Minkowski functionals and we averaged the results over the simulations. Plots of the results are reported in figures 10 - 16.

From the results, we can observe that the parameters which have more influence in the variability of the Minkowski functionals are L, λ and b_2. This should be taken into account in the definition of a more accurate model.

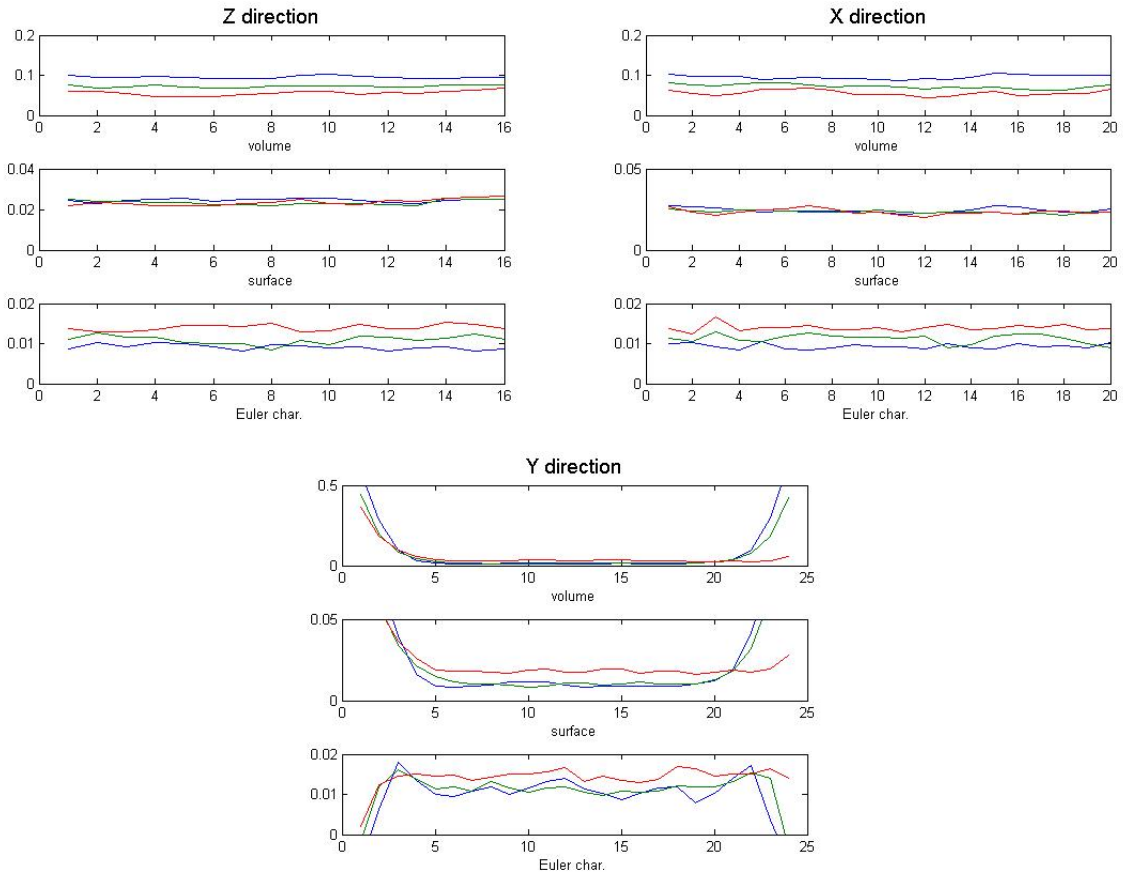

Figure 10: Mean Minkowski functionals computed letting the parameter $nplanes$ vary. Each curve corresponds to a different tested value of $nplanes$

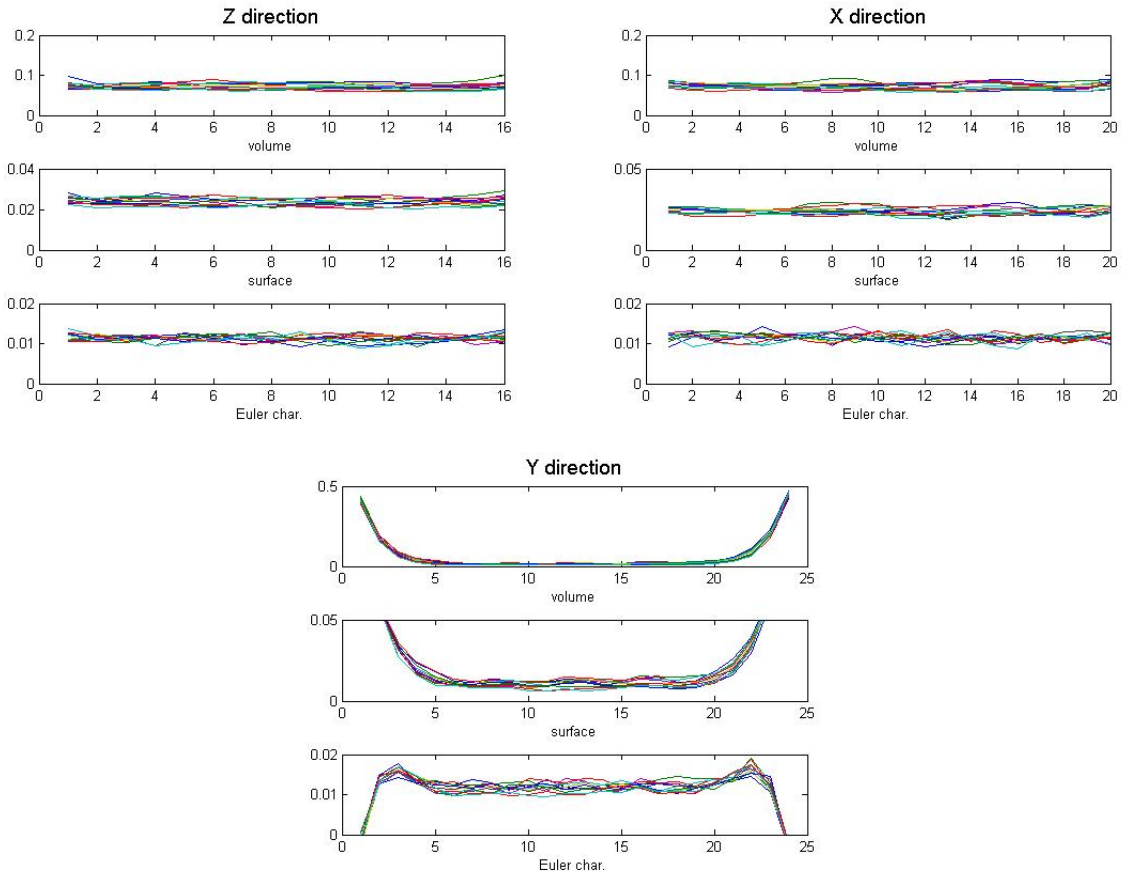

Figure 11: Mean Minkowski functionals computed letting the parameter σ_{hor} vary. Each curve corresponds to a different tested value of σ_{hor}

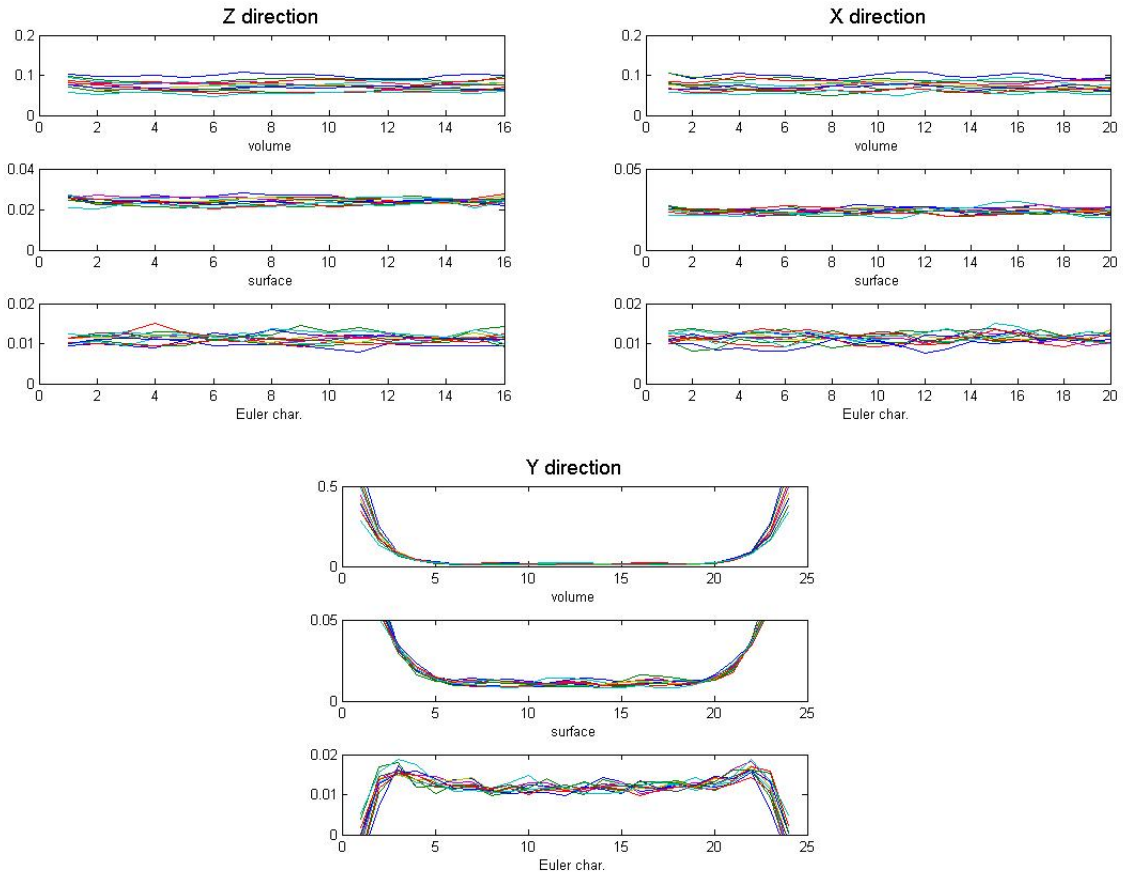

Figure 12: Mean Minkowski functionals computed letting the parameter σ_{vert} vary. Each curve corresponds to a different tested value of σ_{vert}

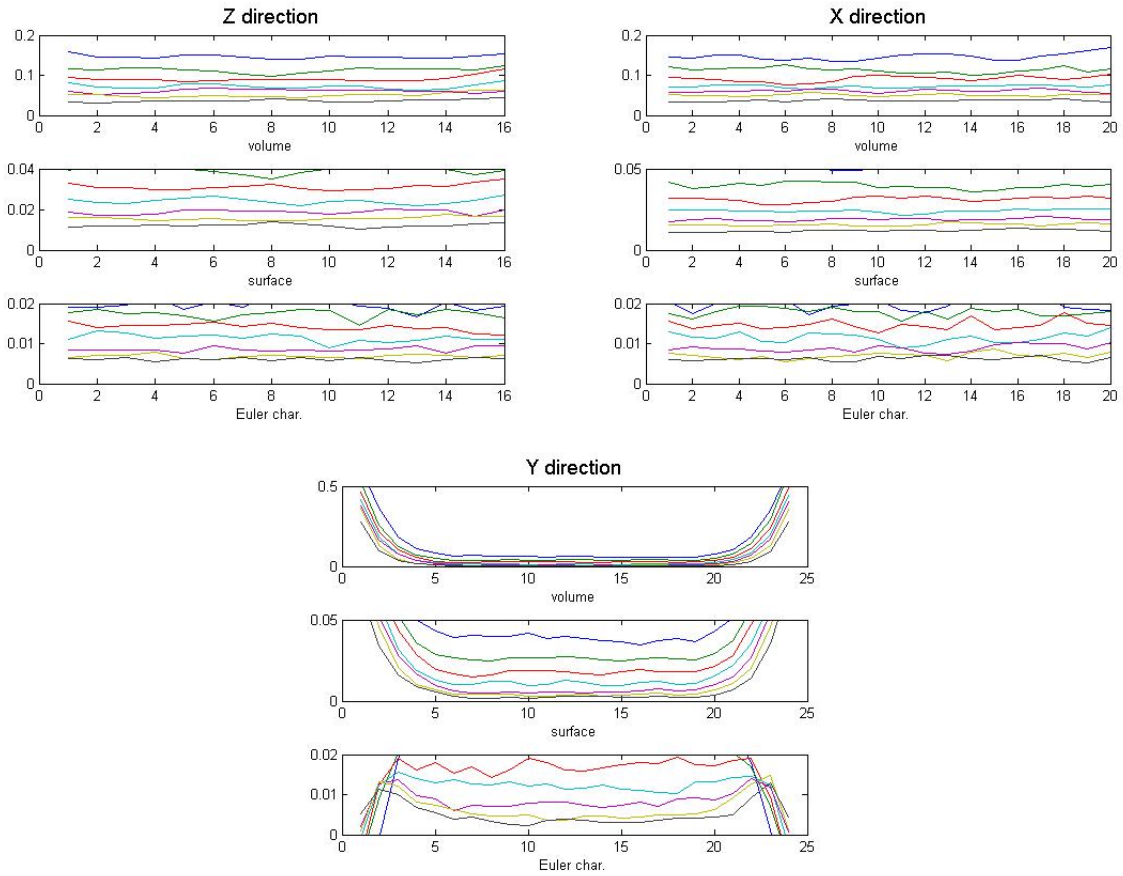

Figure 13: Mean Minkowski functionals computed letting the parameter L vary. Each curve corresponds to a different tested value of L

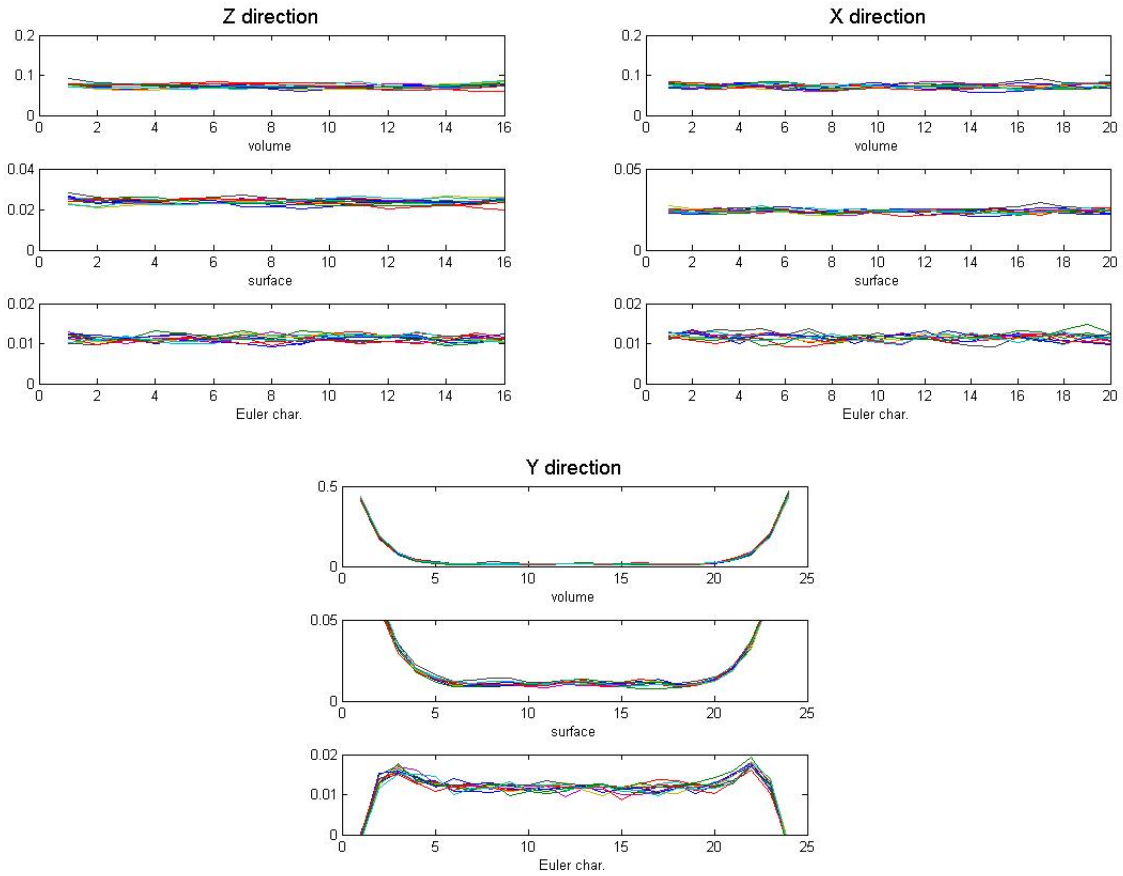

Figure 14: Mean Minkowski functionals computed letting the parameter b_1 vary. Each curve corresponds to a different tested value of b_1

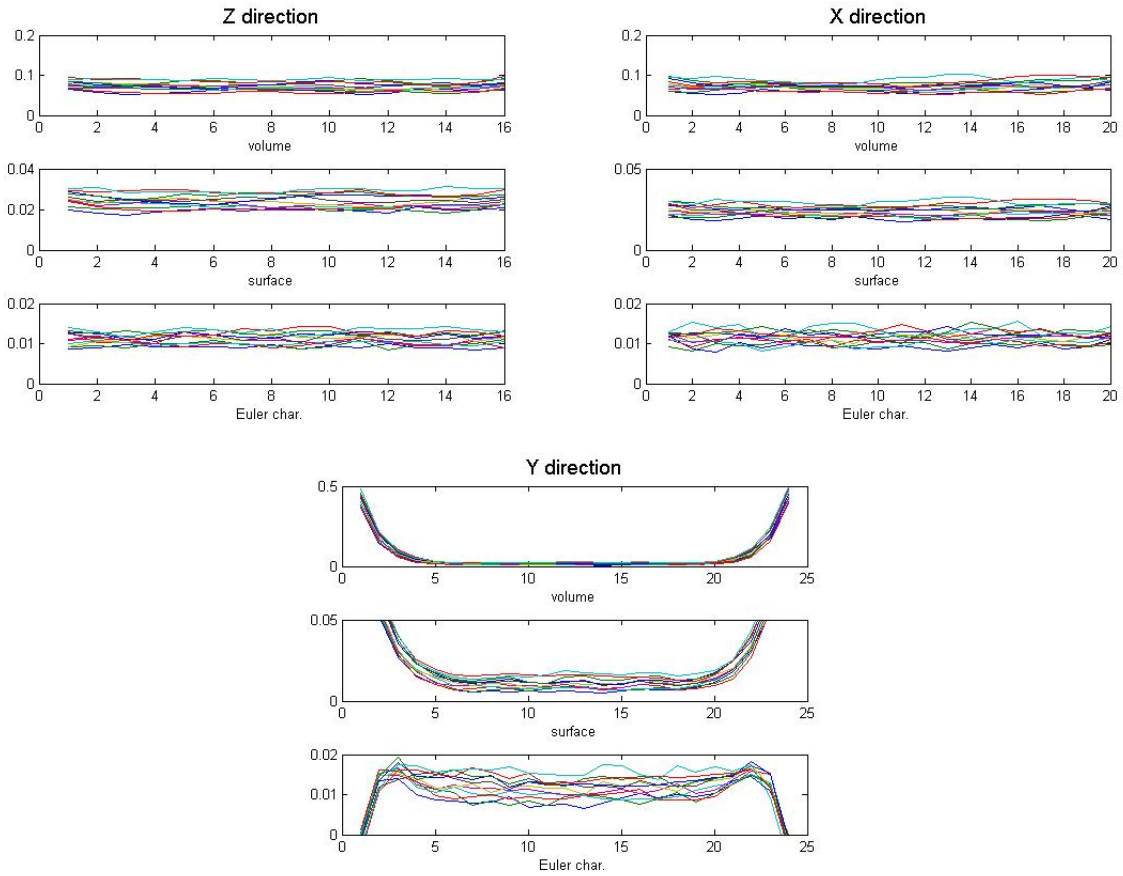

Figure 15: Mean Minkowski functionals computed letting the parameter b_2 vary. Each curve corresponds to a different tested value of b_2

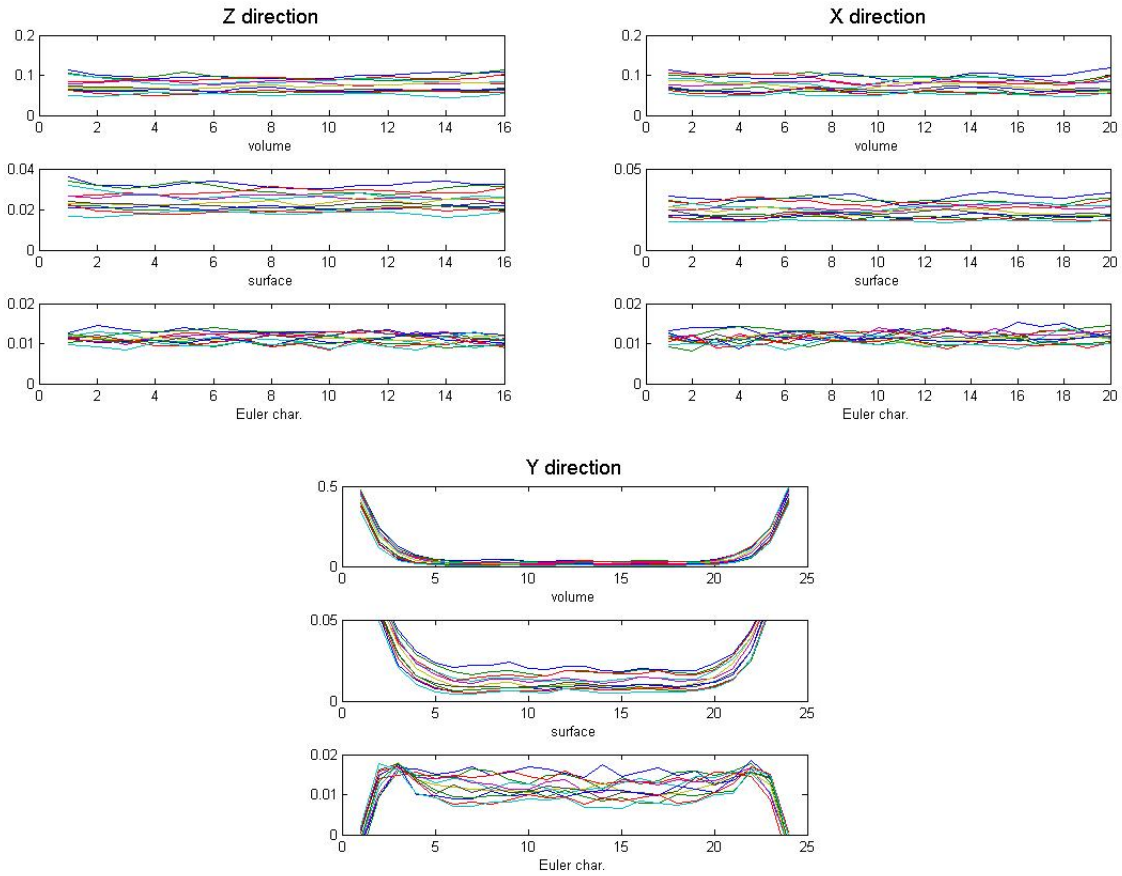

Figure 16: Mean Minkowski functionals computed letting the parameter λ vary. Each curve corresponds to a different tested value of λ

Parameter	optimal value
n_{planes}	15
σ_{hor}	1.2801
σ_{vert}	4.1759
L	18
$b1$	5.1655
$b2$	2.3845
λ	9011

Table 4: Optimal values of the parameters using only 16 sections. The corresponding computed Mahalanobis distance is 1. The simulations have been performed in a parallelepiped having the same dimensions of the real sample in directions X and Y, and dimension 16 in direction Z. The unit of measure of the parameters is a voxel side length

7 Plausibility regions and reduction of the number of sections

Here we propose a technique to quantify the additional uncertainty in the parameter estimates which is introduced when the number of available sections is reduced. When a geometric model able to reproduce in a better way the geometric characteristics of the real sample will be available, this technique can be applied by the industry to fit the model to the data with a desired accuracy.

In order to produce this quantification we computed some *plausibility regions* for the estimated parameters, by fixing a threshold d_{max} on the Mahalanobis distance

$$\Delta(\underline{p}) = \Delta(\underline{S}_{real}, \bar{\underline{S}}_{sim}(\underline{p}))$$

used in the optimization procedure and by computing the convex hull of the points $\underline{p}$ satisfying

$$\Delta(\underline{p}) \leq d_{max}. \tag{2}$$

Since $\underline{p} \in \mathbb{R}^7$, the convex hull will be a polytope in $\mathbb{R}^7$. The increase in variability due to the reduction of the number of sections can be quantified via the ratio of the volumes of the 7-dimensional plausibility regions computed using all sections or a lower number of sections.

Note that the Minkowski functionals can be estimated in a reliable way only if the sections are contiguous, i.e. if their distance is comparable with the side of a pixel.

The variance of the estimated functionals increases when the volume of the region in which they are computed is reduced. This fact causes an increase in the volume of the corresponding plausibility regions when the number of sections is reduced.

As an example, we considered a subset of the real sample composed by 16 consecutive sections (which corresponds about to $1/10$ of the original number of sections of the real sample), resulting thus in a slice of the real sample taken orthogonally to direction Z. We fixed $d_{max} = 3$, and we used our first germ-grain model, with planes located randomly in the Y direction, whose optimal parameters using all sections are reported in Table 1. We estimated the optimal parameters using only 16 sections, and the results are reported in Table 4.

We then fixed $d_{max} = 3$ and computed the volume of the 7-dimensional convex hull of the points satisfying (2), obtaining:

with all sections: $Vol_{all} = 5.0673e + 12$

with 16 sections: $Vol_{16} = 2.4133e + 16$

Thus dividing about by 10 the number of considered sections we obtain a relative increase of variability (i.e. uncertainty) in the parameters estimate of

$$\frac{Vol_{16}}{Vol_{all}} = 4762.$$

Such technique can be used to quantify the increase in variability for different choices of the number and location of the considered sections, thus providing to Nippon Steel & Sumitomo Metal an instrument to evaluate quantitatively the consequences of their choices.

REFERENCES

[1] V. Capasso (ed): Mathematical Modelling for Polymer Processing. Polymerization, Crystallization, Manufacturing. Mathematics in Industry, Vol.2, Springer-Verlag, Heidelberg (2003).

[2] S.N.Chiu, D. Stoyan, W.S. Kendall, J. Mecke, *Stochastic Geometry and its Application. 3rd edition*, John Wiley & Sons, New York (2013).

[3] D. Legland, K. Kieu, M.F. Devaux, Computation of Minkowski measures on 2D and 3D binary images, *Image Anal. Stereol.*, **26**, 83–92 (2007), web: http://www.ias-iss.org/ojs/IAS/article/view/811

[4] http://it.mathworks.com/matlabcentral/fileexchange/33690-geometric-measures-in-2d-3d-images

[5] G. Matheron: *Random Sets and Integral Geometry*. John Wiley & Sons, New York, 1975.

[6] J. Serra, *Image analysis and mathematical morphology*, Volume 1, Academic Press (1982).

[7] P. Suwanpinij, N. Togobytska, U. Prahl, W. Weiss, D. Hömberg, and W. Bleck, Numerical Cooling Strategy Design for Hot Rolled Dual Phase Steel, *Steel Research Int.*, 81, 2010.

[8] E. Villa, P.R. Rios, Transformation kinetics for nucleation on random planes and lines, *Image Anal. Stereol.* **30**, 153–165 (2011)